Spatio-temporal Koopman Decomposition in offshore wind turbines

Soledad Le Clainche[1]*, Xuerui Mao[2], José M. Vega[1]

ISROMAC 2017

International Symposium on Transport Phenomena and Dynamics of Rotating Machinery

Maui, Hawaii

December 16-21, 2017

Abstract

This article presents the spatio-temporal analysis of the flow structures in the wake of an offshore wind turbine using spatio-temporal Koopman decomposition (STKD). STKD is a new method that obtains and combines the main frequencies and wavenumbers (characterizing a specific spatial direction) contained in a flow, with the aim at representing the main flow structures as a whole of traveling waves. The results obtained show that the complex behaviour of the wake of the wind turbine is mainly driven by a single traveling wave moving downstream and a combination of small amplitude traveling waves, related to velocity fluctuations, that represent the flow rotation.

Keywords

Wind turbines — Flow structures — DMD — HODMD — Koopman modes — STKD

[1] *School of Aerospace Engineering, Universidad Politécnica de Madrid, Madrid, Spain*

[2] *University of Nottingham, Nottingham, United Kindom*

*__Corresponding author__: soledad.leclainche@upm.es

INTRODUCTION

The recent knowledge of environmental problems, such as the green-house effect or the hole in the ozone layer, yields the need to increase the use of renewable energies instead of fossil fuels, to produce several types of energy. Offshore wind energy is a type of renewable energy that uses wind power to generate electricity. Due to its good performance, this type of energy has become very popular during the last years. Offshore wind speeds availables are higher than the ones found in land, making this energy more efficient than others and consequently, making profitable the construction of wind farms offshore.

Due to its high complexity, the deep study and understanding of the complex behaviour that takes place in the wake of an offshore wind turbine is a research topic of high interest [1]. Wake interactions in wind farms may lead to highly complex non-linear phenomena that need to be analyzed using sophisticated techniques, such as Spatio-Temporal Koopman Decomposition (STKD)[3]. This technique express the evolution of spatio-temporal flow structures as a whole of traveling waves that moves with a certain phase velocity. In this way, it is possible to simplify very complex flow features, as the ones found in the wake of a wind turbine, and consequently, undestanding the flow behaviour. In this article STKD is applied to study the spatio-temporal flow structures of the wake of an offshore wind turbine.

The article is organized as follows. Section 1 introduce briefly the STKD method. Section 2 presents the model and the performance of the numerical simulations. Finally, Sections 3 and 4 explain the main results and conclusions.

1. SPATIO-TEMPORAL KOOPMAN DECOMPOSITION

Spatio-temporal Koopman decomposition (STKD) is a recently introduced method[3] suitable to study spatio-temporal flow structures. The method combines either singular value decomposition (SVD) [8] or higher order SVD[10] with dyanamic mode decomposition (DMD) [7] or higher order DMD [2] to obtain the main frequencies ω_n and wavenumbers κ_m describing the flow. STKD combines these results to obtain spatio-temporal STKD modes q_{mn} represented by traveling waves, whose phase velocity is defined as $c = -\omega_n/\kappa_m$. Therefore, it is possible to represent highly complex spatio-temporal structures as a whole of traveling waves, helping in this way to understand the reality.

STKD decomposes spatio-temporal data $u(x, y, z, t)$ (where x, y, z and t are the streamwise, normal and spanwise components and t is the time) as a sum of spatio-temporal STKD modes in the following way:

$$u(x, y, z, t) \simeq \sum_{m,n=1}^{M,N} a_{mn} q_{mn}(y, z)\, e^{(\nu_m + i\kappa_m)x + (\delta_n + i\omega_n)t} \quad (1)$$

where ν_m and δ_n are the growth rates related to the spatial and temporal modes, respectively, a_{mn} are the spatio-temporal amplitudes. Spatio-temporal diagrams $\omega - \kappa$, become determined by the value of the spatio-temporal amplitudes. They relate the frequencies and wavenumbers, helping

to understand the flow behaviour, since the main direction and slope of the traveling waves, defined as $\Delta t/\Delta x$, is related to the traveling wave phase velocity as $\Delta t/\Delta = -1/c$.

STKD is applied to a set of spatio-temporal data $u(x, y, z, t)$, equispaced in space Δx and in time Δt, and collected in a tensor as $U(x_i, \boldsymbol{y}, \boldsymbol{z}, t_k)$, for $1 \leq i \leq N_x$ and $1 \leq k \leq K$, with N_x and K as the number or points in the spatial direction and number of temporal snapshots, respectively. The main algorithm considers two main steps, particularized for this problem they read as the following.

- As first step HOSVD is performed to the tensor U in order to clean spatial redudancies, usualy found in data coming from numerical simulations[4], and noise, commonly found in experimental data [5]. HOSVD performs singular value decomposition (SVD) in each one of the spatial directions and combines the results. Hence, the original data tensor is decomposed in spatial modes in x, in y and in z and temporal modes in t. The number or retained SVD mode is established by a tolerace ε, set by the user, determining the root mean square (RMS) error of the approximated solution.

- As second step HODMD is applied to the temporal and spatial SVD modes in t and x, previously obtained. HODMD is a technique that combines classical DMD with Takens' delay embedding theorem [9], using d time-lagged snapshots, reducing not only data uncertainty, but also increasing their accuracy and covering a wider range of applications than DMD. Thus, depending on the case analyzed, using HODMD could be the best option [6]. At this step, the main frequencies and wavenumbers are calculated. The number of retained modes is established by a second tolerace ε_1, also set by the user. In addition, the parameter d for the HODMD analysis is also set by the user, after some calibration, based on the robustness of the results obtained.

2. MODEL DESCRIPTION, NUMERICAL SIMULATIONS AND COMPUTATIONAL DOMAIN

The wake of an offshore turbine has been studied in detail at Reynolds number 1000, defined as Re= $U_\iota D/\nu$, where U_ι is the freestream velocity, D is the diameter of the wind turbine and ν is the kinematic viscosity. To this purpose, three-dimentional numerical simulations have been performed to solve the incompressible non-linearized Navier-Stokes equations in a Cylindrical system. The x-r plane is decomposed into 4722 spectral elements, each of which is further discretized with nodal based Gauss-Labatto-Legendre basis functions with polynomial order 7. In the azimuthal direction, a Fourier decomposition is applied and 96 Fourier modes are calculated.

The computational domain is a cylinder with dimensions $L_x = 63$, $R = 35$, where the wind turbine is located at $(x, r) = (0, 0)$. The wind turbine is modeled using an actuator disc model with unit radius. In this model, the thrust acting on the turbine is considered as uniform over a disk region and therefore a uniform external forcing is added to the momentum equations of the fluid flow in the disk region.

3. FLOW STRUCTURES IN THE WAKE OF THE OFFSHORE WIND TURBINE

The wake of a wind turbine is mainly driven by the big bulk of fluid that travels downstream, following the wind direction, and that is rotating, due to the influence of the wind turbine axis rotation. These two main movements, longitudinal and rotational, make that the description and evolution of velocity fluctuations in the wake of a wind turbine be complex and, consequently, unpredictable and unknown. On the one hand, a good way to simplify reality is studying the flow evolution as a simple combination of traveling waves. To this purpose, it is necessary first, to study the spatio-temporal behaviour of the flow. On the other hand, using the Reynolds decomposition, it is possible to decompose the unsteady, instantaneous, flow field $\boldsymbol{u}(\boldsymbol{x}, t)$ as a combination of the time-averaged flow $\boldsymbol{U}(\boldsymbol{x})$ plus its fluctuations $\boldsymbol{u'}(\boldsymbol{x}, t)$ as $\boldsymbol{u}(\boldsymbol{x}, t) = \boldsymbol{U}(\boldsymbol{x}) + \boldsymbol{u'}(\boldsymbol{x}, t)$.

Figure 1 left shows the spatio-temporal diagram of the streamwise velocity downstream the wind turbine at a representative point of the computational domain. The figure shows three types of flow behaviour. In the near field of the wind turbine ($x/D < 5$) the waves describing the flow are very low intensity and remain standing. In the intermediate field, $5 < x < 13$, the figure suggests that there is a wave traveling along the streamwise direction, with slope $\Delta t/\Delta x \simeq 3/2$. Finally, in the far field, $x > 13$, the flow behaviour changes, but the character of the traveling wave of the previous region still remains. Figure 1 right shows the same spatio-temporal diagram, but, of the streamwise velocity fluctuations. As seen, there is a traveling wave driving the flow along the entire domain represented, with the same slope calculated before. Despite of the fact that it is still possible to distinguish the three regions previously mentioned, the near field and intermediate field are now joined to a single region.

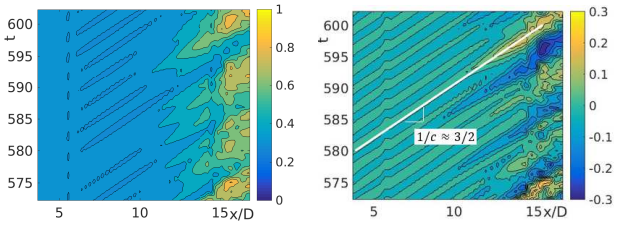

Figure 1. Spatio-temporal diagram along the streamwise direction of the streamwise component at $r/D = 1$ and $\theta = \pi/4$. Left: unsteady flow field u_x. Right: velocity fluctuations u'_x.

Figure 2 shows the normal instantaneous velocity u_y (left), the mean flow (middle) and the velocity fluctuations (right) at two different locations of the computational domain (intermediate and far field) for $0 < r/D < 2$. The instantaneous flow filed shows that it is possible to ditinghish the

rotational character of the flow in the far field, but not in the near-intemediate field. This result is in good agreement with the two regions ditinguished in spatio-temporal diagram of Figure 1 right. This rotational behaviour is driven by the velocity fluctuations, whose mean value is ~ 200 times smaller than the value of the mean flow in the near field ($x/D < 6$ and ~ 30 times smaller considering also the far field ($0 < x < 18$). The same behaviour is described by the velocity u_z, but phase-shifted π radians, not shown for the shake of brevity.

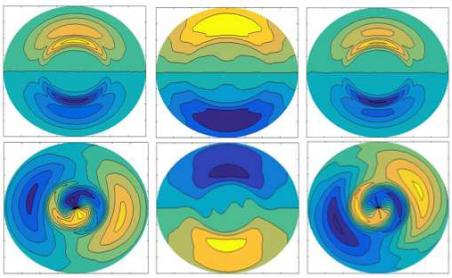

Figure 2. Radial velocity at $x/D = 6$ (top) and $x/D = 18$ (bottom). From left to righ: instantaneous field u_y, time-averaged value U_y and velocity fluctuations u'_y.

STKD analysis has been performed to the three components of the instantaneous velocity in a smaller region of the computational domain, defined in Figure 3. The Figure also shows the evolution of the streamwise velocity fluctuations along the streamwise component. As seen, the intensity value of the velocity fluctuations is very small near the wind turbine but increases with x/D. The analysis has been performed in the region where the value of the main fluctuations start growing ($3.5 < x < 18$), since, as shown in Figures 1 and 2, they are carrying the traveling waves. The analysis performed is three-dimensional, with the aim at findind the two-dimenstional modes related to the main traveling waves that move along the stremwise direction, with phase velocity $c = -\omega_n/\kappa_m$. A set of 100 snapshots, equispaced in time $\Delta t = 0.2$, has been used in the temporal STKD analysis, while a set of 240 points, equispaced in space along the streamwise direction $\Delta x = 5.8543 \cdot 10^{-2}$, is used for the spatial analysis. The parameters used for this analysis are $d_t = 20$ and $d_s = 40$, for the spatial and temporal analysis, respectively, and the toleraces are set to $\varepsilon = \varepsilon_1 = 0.01$.

Figure 4 shows the frequencies and wavenumbers as function of their amplitudes. STKD captures two temporal modes with $\omega = 0$ related to the mean flow (mode with largest amplitude) and its correction, and a single mode with frequency $\omega_1 \simeq 2$. Similar results are obtained for the spatial analysis, where two modes with $\kappa = 0$ and a mode with $\kappa_1 \simeq 3$ are found describing the flow. Figure 5 left shows the spatio-temporal diagram that relates the wavenumbers and frequencies previously obtained. The number of spatio-temporal modes retained is 4 (2 steady modes and a mode with frequency/wavenumber and its conjugate complex mode). As seen in the Figure, there is a traveling wave describing the

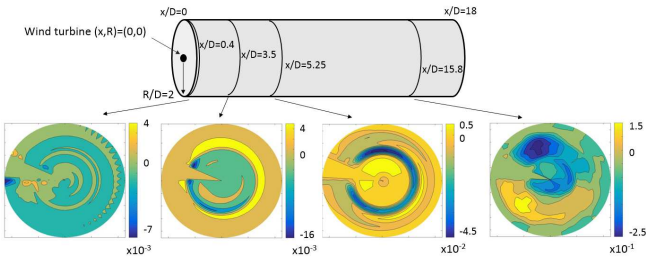

Figure 3. Computational domain for STKD analysis. Contours of streamwise velocity fluctuations along the streamwise component.

flow, with phase velocity $c = -\omega_1/\kappa_1 \simeq 2/3$. The existence of this traveling wave was already predicted in Figure 1. Figure 5 right shows the reconstruction of the instananeous streamwise velocity using the spatio-temporal modes, whose RMS error is $\sim 1.58 \cdot 10^{-1}$. The traveling wave is perfectly identified, however, the intensity level of the reconstruction is smaller than the original field, and the complex behaviour related to the velocity fluctuations is missing.

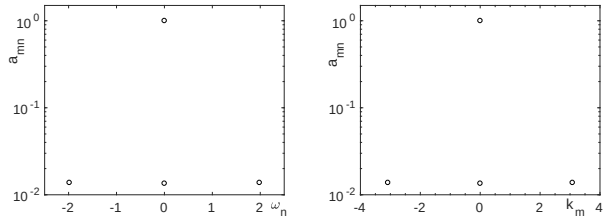

Figure 4. STKD analysis of the instantaneous flow field with tolerances $\varepsilon = \varepsilon_1 = 0.01$. From left to right: frequencies and wavenumbers as function of their amplitudes.

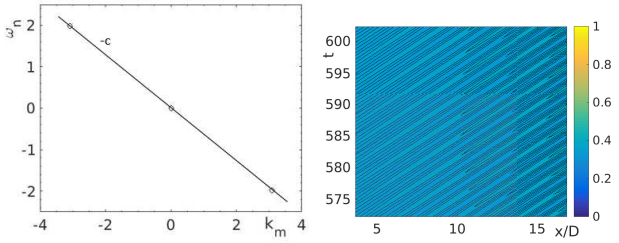

Figure 5. STKD analysis of the instantaneous flow field with tolerances $\varepsilon = \varepsilon_1 = 0.01$. Left: spatio-temporal diagram. Right: reconstruction of the original flow field.

The same analysis have been perfomed decrasing the tolerance to $\varepsilon = \varepsilon_1 = 5 \cdot 10^{-3}$. STKD captures now 66 spatio-temporal modes, including the modes corresponding to the traveling wave and the mean flow. However, the reconstruction RMS error has only been decreased to $\sim 1.43 \cdot 10^{-1}$, meaning that velocity fluctuations are modeling the flow behaviour. Thus, with the aim at capturing more in detail the flow behaviour, two possible STKD analysis could be performed instead. As first option, it is possible to analyze

the instananeous flow field substracting the reconstruction previously obtained (mean flow and main traveling wave). As second option, the analysis could be directly performed to the velocity fluctuations.

Firstly, STKD analysis has been performed to the result obtained when the traveling wave and the mean flow are substracted to the instantaneous flow field, shown in Figure 6 top left. The parameters used in previous analyses are maintained, but the tolerances are increased to $\varepsilon = \varepsilon_1 = 1 \cdot 10^{-1}$, since the differences in the amplitude of the modes are now smaller (fluctuations around the main flow). STKD retains 100 spatio-temporal modes with reconstruction RMS error $5.1 \cdot 10^{-1}$. Figure 6 shows the reconstruction using such 100 spatio temporal modes (top right), the frequencies and wavenumbers as function of their amplitudes (bottom left and middle) and the spatio-temporal diagram (bottom right). On the one hand, the reconstructed flow field captures some of the main features of the original one, but it would be necessary to retain a larger number of modes to improve the solution. On the other hand, the method retains a large number of frequencies and wavenumbers, so it is difficult to identify the more relevants. The spatio-temporal diagram shows several frequency-wavenumber combinations, in good agreement with the high complexity of this flow, that could be represented as a combination of multiple traveling waves. However, the simplest solution represents the flow as a combination of standing waves (horizontal lines with $\omega_n = 2, 1, 0, -1, -2$), modulated (the remaining horizontal lines). The method give accurate reconstruction of the flow field, however, the flow physics related to the wind turbine rotation might difficult to understand from the results obtained.

Secondly, STKD has been performed to the velocity fluctuations. The parameters used for the previous analyses are maintained, but, as in the previous case, the tolerances are increased to $\varepsilon = \varepsilon_1 = 1 \cdot 10^{-1}$ for similar reasons as in the former case. Figure 7 shows the frequencies and wavenumbers as function of the spatio-temporal amplitudes obtained for this analysis. As seen, there is a dominant frequency and wavenumber, $\omega_1 \simeq 2$ and $\kappa_1 \simeq 3$, respectively. These results are in good agreement with the one obtained in the analysis of the instantaneous flow field. The spatio-temporal diagram of Figure 8 top left shows the 14 spatio-temporal modes retained for this analysis (7 modes and their conjugate complex). The diagram shows that it is possible to describe the flow as a sum of traveling waves, with very similar positive slopes. The main traveling wave with phase velocity $c = 2/3$, previously obtained, is also identified in the diagram. The reconstruction of the flow field, whose RMS error is $5.02 \cdot 10^{-1}$, is shown Figure 8 top left. As in the analysis performed in the instantaneous flow field, it is possible to identify the structure of the main traveling wave, but the structure is now slightly more complex, due to the influence of the lower amplitude traveling waves (obtained from the diagrams of Figure 7). With the aim at studying more in depth the evolution of the velocity fluctuations, the same analysis has been performed descreasing the tolerance to $\varepsilon_1 = 5 \cdot 10^{-2}$. Figure 8 bottom shows the results obtained. The spatio-temporal diagram shows the 44 spatio-temporal modes retained (22 modes and their complex cojuated). Again, the main traveling wave is identified, and some other lower amplitude traveling waves with positive and negative slope. The negative slope traveling waves represent the flow field traveling in oposite direction. This fact suggests that the rotational movement of the flow along the streamwise axis, may invoke unexpected movements of the very small and low intensity flow scales. The reconstructed flow field, with RMS error $4.99 \cdot 10^{-1}$, matches better the original solution than in the preivous case. Especially at points $x/D > 13$. Retaining a larger number of traveling waves (positive and negative slopes), the rotational movement of the flow, driving this region, is better recovered. Nevertheless, the reconstruction error is almost the same as in the former case, meaning that these additional modes are very low amplitude ones.

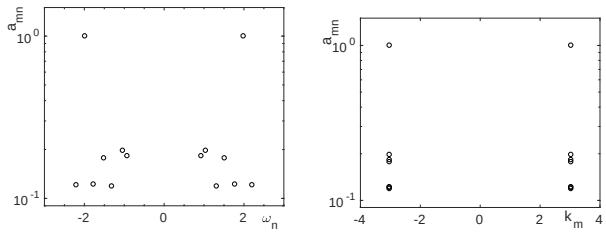

Figure 7. Counterpart of Figure 7 for the velocity fluctuations analysis using $\varepsilon = \varepsilon_1 = 1 \cdot 10^{-1}$.

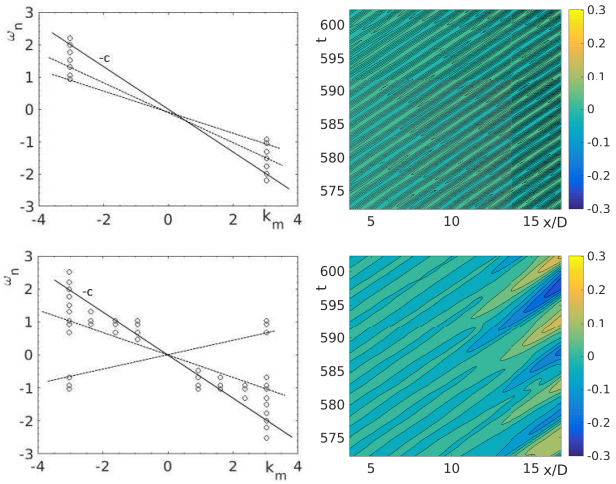

Figure 8. Counterpart of Figure 5 for the velocity fluctuations analysis using $\varepsilon = \varepsilon_1 = 1 \cdot 10^{-1}$ (top) and $\varepsilon = 1 \cdot 10^{-1}$, $\varepsilon_1 = 5 \cdot 10^{-2}$ (bottom).

Finally, Figure 9 shows the spatio-temporal modes obtained in this analysis, shown in Figure 8 top left. The modes are ordered from highest to lowest amplitude. As seen, the first mode, that represents the main traveling wave ($c = 2/3$), is uniform in the streamwise component, and in the remaining components, presents a reflection symmetry with respect

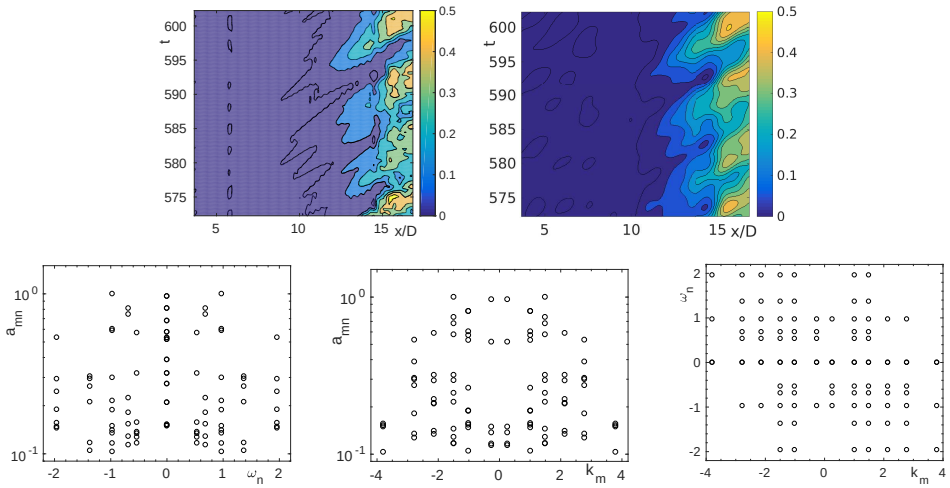

Figure 6. Top: Result of the streamwise instantaneous velocity substracting the traveling wave shown in Figure 5 (left) and its reconstruction (right) using the spatio-temporal modes obtained with STKD shown in the bottom of this Figure. Bottom: From left to right, frequencies and wavenumbers as function od the spatio-temporal amplitudes and the spatio-temporal diagram obtained with STKD and $\varepsilon = \varepsilon_1 = 1 \cdot 10^{-1}$.

to the vertical and horizontal axis, in the origin. In the remaining modes, the streamwise component is not uniform, but presents groups or disorganized structures. The remaining components, preserve the symmetry with respect to the origin, but the structures are now rotated. Additionally, it is possible to distinguish the rotational movement within these modes, related to the flow structures shown in Figure 2. However, a more sophisticated STKD analysis should be performed in the azimuthal component in order to identify the direction of rotation of the identified flow structures. But this is far from the scope of this article. Lastly, it is remarkable that, in all the modes presented, the real part of the streamwise component shows a region with negative value at $r/D \sim 1$, suggesting that the wind turbine foils may produce a very slight suction movement trough the velocity flctuations, probably related to the rotation of the flow field.

4. CONCLUSIONS

Flow structures in the wake of an offshore wind turbine have been studied in detail using a new method, STKD. This method combines either SVD or HOSVD with either DMD or HODMD to perform spatio-temporal analyses, obtaining as result the main frequencies and wavenumbers contained in a flow, and their combination. Thus, highly complex spatio-temporal structures, as the ones found in the wake of an offshore wind turbine, can be understood as a whole of traveling waves, whose phase velocity is determined by the combination of frequencies and wavenumbers. The main results show that the flow is mainly driven by a single traveling wave with phase velocity $c = 2/3$, moving in the wind direction. However, due to both, the rotational movement of the flow traveling downstream, and the complex movement of the velocity fluctuations, it is necessary to include additional flow strucures to describe the complete flow behaviour. These flow features become represented by lower amplitude traveling waves with phase velocity very similar to the driven traveling wave, or even with negative phase velocity, representing the strongest rotation regions. These results shed light on undertanding the complex behaviour found in the wake of a wind turbine, very useful to predict the effects produced in the interaction of the wake with another wind turbine.

ACKNOWLEDGMENTS

This work was partially supported by the Spanish Ministry of Economy and Competitiveness, under grant TRA2016-75075-R.

REFERENCES

[1] Ferrer, E. & Le Clainche, S. 2015 Flow scales in cross flow turbines *Book chapter in CFD for Wind and Tidal Offshore Turbines, Springer Tracts in Mechanical Engineering, ISBN 978-3-319-16201-0*, 1–11.

[2] Le Clainche, S. & Vega, J.M. 2017 Higher order dynamic mode decomposition. *SIAM J. on Appl. Dyn. Sys.* **16(2)**, 882–925.

[3] Le Clainche, S. & Vega, J.M. 2017 Spatio-temporal Koopman decomposition. *Submitted to J. of Nonlin. Sci.*

[4] Le Clainche, S. & Vega, J.M. 2017 Higher order dynamic mode decomposition to identify flow patterns and extrapolation properties. *Phys. of Fluids* **29(8)** 084102

[5] Le Clainche, S., Sastre, F., Vega, J.M., Velazquez, A. 2017 Higher order dynamic mode decomposition applied to study flow structures in noisy PIV experimental data *AIAA 2017-3304 . Proceedings of 47th AIAA Fluid Dynamics Conference, 5 – 9 June, Denver, CO, USA.*

[6] Le Clainche, S., Vega, J.M. & Soria, J. 2017 Higher order dynamic mode decomposition for noisy experimental data: the flow structure of a zero-net-mass-flux jet. *Exp. Therm. and Fluid Science* **88**, 336–353

[7] Schmid, P.J. 2010 Dynamic mode decomposition of numerical and experimental data. *J. Fluid Mech.* **656**, 5–28.

[8] Sirovich, L. 1987 Turbulence and the dynamic of coherent structures, parts I–III. *Q. Appl. Math.* **45** (3), 561.

[9] Takens, F. 1981 Detecting strange attractors in turbulence, *Lecture Notes in Mathematics, D.A. Rand and L.-S. Young. eds., Springer-Verlag*, pp. 366–381.

[10] Tucker, L.R. 1996 Some mathematical notes on three-mode factor analysis. *Psikometrica*, **31**, 279–311.

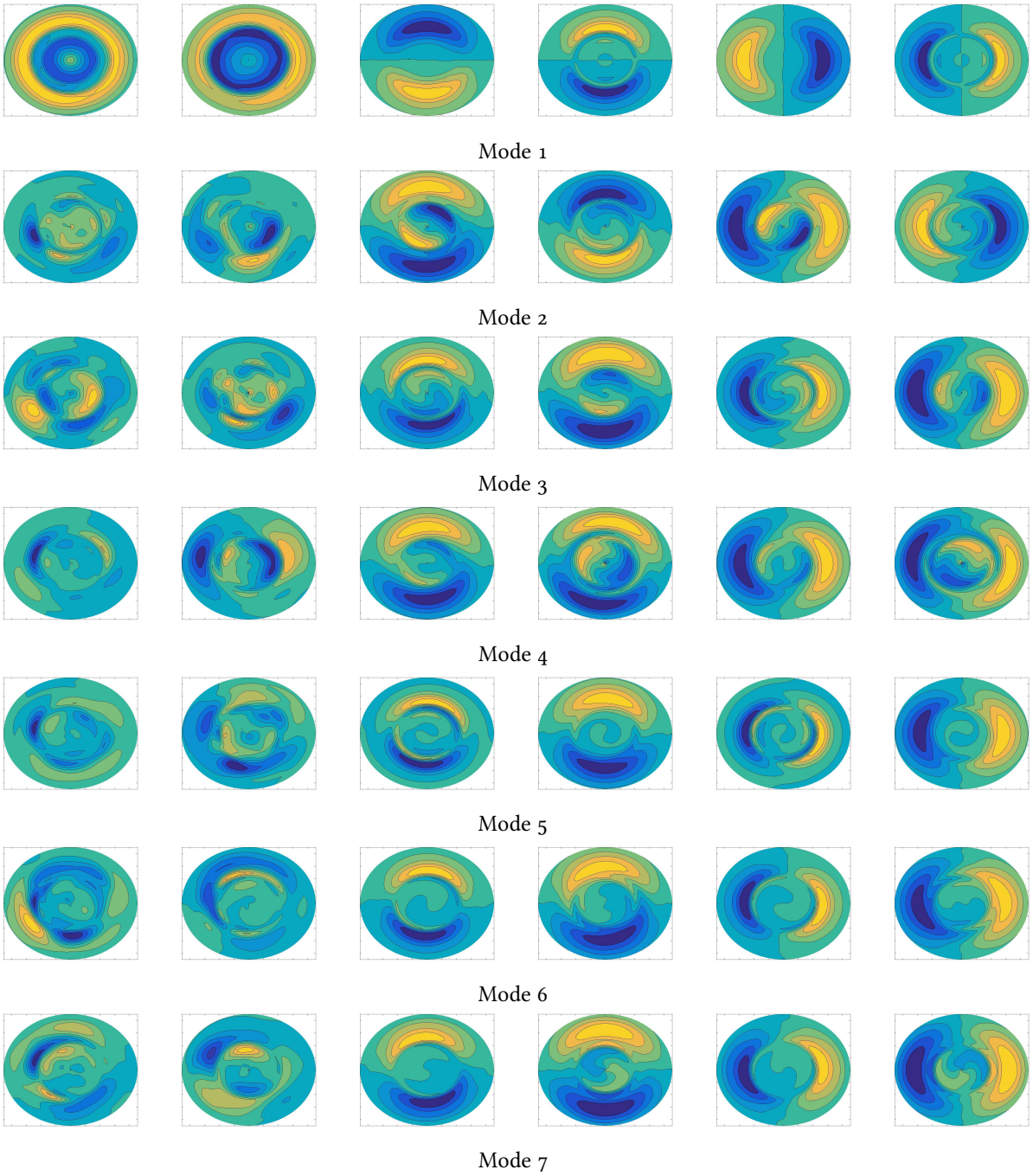

Figure 9. Spatio-temporal modes represented in the $\omega - \kappa$ diagram of Figure 8 top left. From left to right: $\mathfrak{R}(u_x)$, $\mathfrak{I}(u_x)$,$\mathfrak{R}(u_y)$, $\mathfrak{I}(u_y)$,$\mathfrak{R}(u_z)$, $\mathfrak{I}(u_z)$.